Computational Fluid Dynamics JOURNAL 12(3):57 October 2003 (pp.475-481)

NUMERICAL SIMULATION OF DROPS IN A SHEAR FLOW BY A LATTICE-BOLTZMANN BINARY FLUID MODEL

Naoki Takada†, Akio Tomiyama‡, Shigeo Hosokawa‡

Abstract

For simulating immiscible two-phase flows and realizing the easy adjustment of surface tension and interface thickness to desired values, a lattice-Boltzmann binary fluid model is improved by (a) the adoption of a particle number density function at a local equilibrium state for the convection term of the lattice Boltzmann equation and (b) the introduction of two parameters in a surface free energy. Neutrally-buoyant drops in simple shear flows are simulated using the improved method to examine its accuracy and characteristics of drop breakup. As a result, it is confirmed that (1) the method can give good predictions for deformation and breakup of single drops and (2) the critical Reynolds number at which drop breakup takes place depends not only on the capillary number and the number density of drops but also on the initial spatial arrangement of drops.

Key Words: Lattice Boltzmann Method, Binary Fluid Model, Drop, Free Energy

1 INTRODUCTION

The lattice Boltzmann method, LBM [1][2], has been developed as an alternative approach for simulating incompressible fluid flows from a statistical-thermodynamic point of view such that collisions and translations of microscopic particles represented by a particle number density function result in a local equilibrium state corresponding to a macroscopic fluid motion. The main advantages of LBM, which are originated from the lattice gas cellular automaton [3], are the easiness in the implementation of boundary conditions for complex geometry, the high efficiency in parallel computing, and the spontaneous formation of fluid-fluid interface. These benefits result from the kinetic equations of particles consisting of a rectilinear convection (or streaming) operator, a local collision operator and a repulsive interaction between particles. Macroscopic variables in the continuum fluid dynamics are obtained by averaging the particle number density functions. The validity of LBM equations and the macroscopic variables is supported by the fact that the continuity and Navier-Stokes equations are recovered by applying the Chapman-Enskog expansion to the LBM equations. Unlike conventional numerical methods based on the continuum equations, the pressure in LBM is also obtained by averaging the number densities so that there is no need to solve a CPU-time-consuming Poisson equation.

Lattice Boltzmann methods based on a free energy theory have been applied not only to one-component vapor-liquid flows [4],[5] but also to two-component binary fluid flows [6],[7]. Hereafter the LBM for binary fluids is referred to as the BF model. The free energy theory has been also utilized in several numerical methods based on the continuum equations such as second gradient methods [8] and phase-field methods [9]. The main reason why the free energy is introduced for simulating two-phase flows is that fluid-fluid interfaces with accurate surface tension force are spontaneously formed by the surface free energy, which in turn means that no interface tracking schemes and no surface tension force models are required for tracking the interface. The LBM based on BF therefore possesses a large potential of simulating complex deformation of multiple interfaces easily and efficiently.

Since the conventional BF model cannot keep the interface thickness small due to a sort of numerical diffusion of number density functions, a simple but effective scheme to keep the interface thickness within a couple of grids is proposed in this study. In addition, the proposed scheme enables us to easily adjust the value of surface tension. The improved lattice-Boltzmann BF model is applied to motions of

Received on August 26, 2003.

† National Institute of Advanced Industrial Science and Technology (AIST), Onogawa, Tsukuba 305-8569, Japan naoki-takada@aist.go.jp

‡ Faculty of Engineering, Kobe University, Rokkodai, Nada, Kobe 657-8501,Japan tomiyama@mech.kobe-u.ac.jp

neutrally-buoyant drops in a shear flow between two parallel plates moving in opposite directions. Predicted deformation and breakup of drops are compared with available data [10],[11] to verify the accuracy of the proposed method.

2 LATTICE-BOLTZMANN BINARY FLUID MODEL

In the binary fluid (BF) model [6], a repulsive interaction between two kinds of fluid particle components A and B is taken into account by using a free energy. Two independent macroscopic variables are introduced to compute pressure and phase distributions, i.e. the total number density $n = n_A + n_B$, and its difference $\Delta n = n_A - n_B$. These variables are evaluated by using two velocity distribution functions for particle number densities, f_a and g_a, where the subscript a denotes the label to distinguish the particles by their velocity vectors $\mathbf{e}_a$. The variables, n, Δn, and the macroscopic flow velocity $\mathbf{u}$ are defined as follows:

$$n = \sum\nolimits_a f_a = \sum\nolimits_a f_a^{eq}, \tag{1}$$

$$\Delta n = \sum\nolimits_a g_a = \sum\nolimits_a g_a^{eq}, \tag{2}$$

$$n\,\mathbf{u} = \sum\nolimits_a f_a\,\mathbf{e}_a = \sum\nolimits_a f_a^{eq}\mathbf{e}_a, \tag{3}$$

$$\Delta n\,\mathbf{u} = \sum\nolimits_a g_a^{eq}\mathbf{e}_a, \tag{4}$$

where the superscript eq denotes a local equilibrium distribution. The total density n is proportional to pressure and approximately constant in a whole flow field, while the density difference Δn takes either positive or negative values in each phase and then represents phase distributions.

Time evolution of f_a and g_a is predicted by the following lattice Boltzmann equations (LBE):

$$\frac{\partial f_a(t,\mathbf{r})}{\partial t} + \mathbf{e}_a \cdot \nabla f_a(t,\mathbf{r}) = -\frac{1}{\tau_1}\left[f_a(t,\mathbf{r}) - f_a^{eq}(t,\mathbf{r})\right] \tag{5}$$

$$\frac{\partial g_a(t,\mathbf{r})}{\partial t} + \mathbf{e}_a \cdot \nabla g_a(t,\mathbf{r}) = -\frac{1}{\tau_2}\left[g_a(t,\mathbf{r}) - g_a^{eq}(t,\mathbf{r})\right] \tag{6}$$

where $\mathbf{r}$ is the position vector, τ_1 and τ_2 are the relaxation times. After collision at a site $\mathbf{r}$, the particles with $\mathbf{e}_a$ move to its neighbor $\mathbf{r}+\mathbf{e}_a$ during unit time period. The terms on the right hand sides of Eqs.(5) and (6), the so-called lattice BGK collision operators [2], represent the relaxation process toward the local equilibrium states f_a^{eq} and g_a^{eq}. The macroscopic variables, n, Δn, and $n\,\mathbf{u}$, are conserved at each site in every collision step.

The thermodynamic behavior of binary fluid system is described by a simple free energy Ψ which accounts for the contribution of surface free energy due to a density gradient [6]:

$$\Psi = \int d\mathbf{r}\left\{\psi(T,n,\Delta n) + \frac{\kappa}{2}\left|\nabla\Delta n\right|^2\right\}, \tag{7}$$

$$\psi = \frac{T_C}{2}\left(n - \frac{\Delta n^2}{n}\right) - nT + \frac{T}{2}\left[(n+\Delta n)\ln\left(\frac{n+\Delta n}{2}\right) + (n-\Delta n)\ln\left(\frac{n-\Delta n}{2}\right)\right], \tag{8}$$

where κ is the capillary coefficient to adjust the magnitudes of surface tension and interfacial thickness, and T_C is the critical temperature. When $T < T_C$, a phase separation automatically takes place in binary fluids under an isothermal condition, i.e., the formation of a component-A-rich and a component-B-rich region results in the separation of two phases.

The function Ψ is related with the pressure tensor $P_{\alpha\beta}$ and the chemical potential difference $\Delta\mu$:

$$P_{\alpha\beta} = P\delta_{\alpha\beta} + \kappa\frac{\partial\Delta n}{\partial x_\alpha}\frac{\partial\Delta n}{\partial x_\beta}, \tag{9}$$

$$P = \Delta n\frac{\delta\psi}{\delta\Delta n} - \Psi = nT - \kappa\left(\Delta n\nabla^2\Delta n + \frac{\left|\nabla\Delta n\right|^2}{2}\right), \tag{10}$$

$$\Delta\mu = \frac{\delta\Psi}{\delta\Delta n} = -T_C\frac{\Delta n}{n}$$

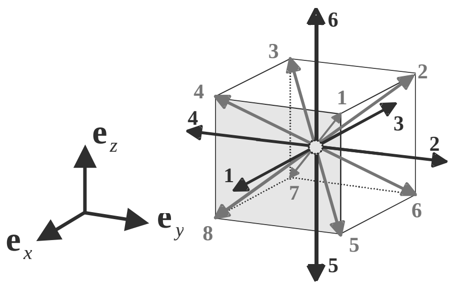

Fig.1: A three-dimensional 15-velocity model.

$$+\frac{T}{2}\ln\left(\frac{1+\Delta n/n}{1-\Delta n/n}\right)-\kappa\nabla^2(\Delta n), \quad (11)$$

where the Greek subscripts are Cartesian coordinate indices and $\delta_{\alpha\beta}$ is the Kronecker's delta. These thermodynamic quantities are embedded into the equilibrium velocity distributions f_a^{eq} and g_a^{eq} as follows:

$$P_{\alpha\beta}=\sum\nolimits_a f_a^{eq}\left(e_{a\,\alpha}-u_\alpha\right)\left(e_{a\,\beta}-u_\beta\right), \quad (12)$$

$$\Gamma\Delta\mu\delta_{\alpha\beta}=\sum\nolimits_a g_a^{eq}\left(e_{a\alpha}-u_\alpha\right)\left(e_{a\beta}-u_\beta\right), \quad (13)$$

where Γ is the parameter corresponding to mobility.

Applying the Chapman-Enskog's multi-scale expansion [2] to Eqs. (5)-(13) yields a complete equation set of continuum fluid dynamics for two-phase fluids [6].

3 3D EQUILIBRIUM DISTRIBUTION OF PARTICLES

An isotropic velocity set including a rest particle component shown in Fig.1 is adopted for $\mathbf{e}_a$ [12]. In this section, the subscript a is replaced with l and i, where l (=1 or 2) is the index of two speeds $c(l+1)^{1/l}$ and i is the index of velocity directions: i=1 to 6 for l=1, i=1 to 8 for l=2. The coefficient c is set to be equal to 1.

Under a low Mach number condition, $f_{l,i}^{eq}$ and $g_{l,i}^{eq}$ are given by [13]

$$f_{li}^{eq}=n\left[A_l+\frac{B_l}{c^2}\mathbf{e}_{li}\cdot\mathbf{u}+\frac{C_l}{c^4}\left(\mathbf{e}_{li}\cdot\mathbf{u}\right)^2+\frac{D_l}{c^2}\mathbf{u}\cdot\mathbf{u}\right] + G_{\alpha\beta}^{(l)}e_{li\alpha}e_{li\beta}, \quad (14)$$

$$f_0^{eq}=n\left[A_0+\frac{D_0}{c^2}\left(\mathbf{u}\cdot\mathbf{u}\right)\right], \quad (15)$$

$$g_{li}^{eq}=\frac{B_l\Gamma\Delta\mu}{c^2}+\Delta n\left[\frac{B_l}{c^2}\left(\mathbf{e}_{l\,i}\cdot\mathbf{u}\right)+\frac{C_l}{c^4}\left(\mathbf{e}_{l\,i}\cdot\mathbf{u}\right)^2+\frac{D_l}{c^2}\left(\mathbf{u}\cdot\mathbf{u}\right)\right], \quad (16)$$

$$g_0^{eq}=\Delta n-\frac{6B_1+8B_2}{c^2}\Gamma\Delta\mu+\frac{D_0}{c^2}\Delta n\left(\mathbf{u}\cdot\mathbf{u}\right), \quad (17)$$

where Eqs.(15) and (17) correspond to the distribution functions for rest particles. The parameters A_l, B_l, C_l, D_l and $G_{\alpha\beta}^{(l)}$ have been determined so as to yield correct continuum fluid equations [13]. The A_l (l=1,2), A_0 and $G_{\alpha\beta}^{(l)}$ (l=1,2) are given by

$$A_l=\frac{s_l}{8\left(s_1+s_2\right)c^2}\left[T-\kappa\frac{\Delta n}{n}\nabla^2\Delta n\right], \quad (18)$$

$$A_0=1-6A_1-8A_2, \quad (19)$$

$$G_{\alpha\beta}^{(l)}=\frac{\kappa}{c^4}\left[E_l\frac{\partial\,\Delta n}{\partial\,r_\alpha}\frac{\partial\,\Delta n}{\partial\,r_\beta}+F_l\left|\nabla\Delta n\right|^2\delta_{\alpha\beta}\right]. \quad (20)$$

Here the fluid temperature T is given by

$$T=8\left(s_1+s_2\right)c^2. \quad (21)$$

where s_1 and s_2 denote the probabilities of presence of particles with speed $2c$ and $\sqrt{3}c$, respectively, under a thermodynamic equilibrium condition.

The following set of parameters are used: B_1= 1/24, B_2= 1/12, C_1= 1/32, C_2= 1/16, D_0= -7/24, D_1= -1/48, D_2= -1/24, E_1 = 1/32, F_1 = -1/32, E_2 = 1/16, and F_2= 0.

4 IMPROVEMENT OF BINARY FLUID MODEL

The BF model is improved to simulate immiscible two phase flows with the function of easy adjustment of surface tension and interface thickness to desired values. First, g_a in the convection term in Eq.(6) is replaced with g_a^{eq}, by which significant reduction of Δn diffusion inherent to the original BF model[6] is achieved:

$$\frac{\partial\,g_a\left(t,\mathbf{r}\right)}{\partial\,t}+\mathbf{e}_a\cdot\nabla g_a^{eq}\left(t,\mathbf{r}\right)$$

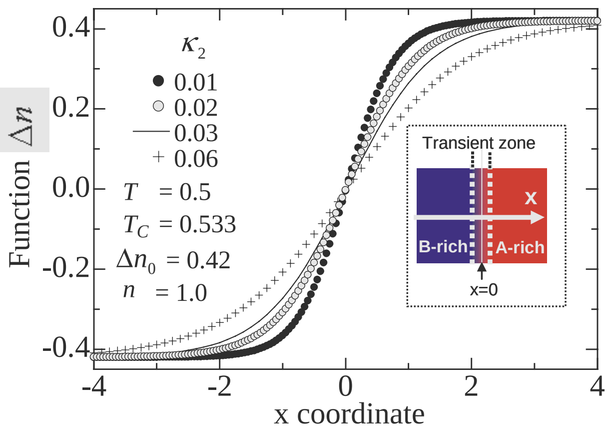

Fig.2: Examples of Δn across a flat interface calculated by using Eq.(24).

$$= -\frac{g_a\left(t,\mathbf{r}\right) - g_a^{eq}\left(t,\mathbf{r}\right)}{\tau_2}. \quad (22)$$

where τ_2 takes a value equal to the time step Δt.

Second, two parameters κ_1 and κ_2 are introduced in the pressure tensor and the chemical potential difference, Eqs. (9) and (11), respectively, instead of the single capillary coefficient κ.

When we carry out a simulation of a given two-phase flow, we must adjust the values of κ_1 and κ_2 so as to make the value of surface tension σ in the simulation equal to that for the given two-phase fluids. If the phase interface is flat and perpendicular to x axis in Cartesian coordinates, σ in a simulation is given as a function of κ_1 and Δn:

$$\begin{aligned}\sigma &\equiv \int_{-\infty}^{+\infty} \left(P_N - P_L\right) dx \\ &= \kappa_1 \int_{-\infty}^{+\infty} \left(\frac{\partial\,\Delta n}{\partial\, x}\right)^2 dx, \quad (23)\end{aligned}$$

where $P_N = P_{xx}$ and $P_L = P_{yy} = P_{zz}$. The density difference $\Delta n(x)$ in Eq. (23) can be evaluated by solving the following equations, which are valid under the condition of constant chemical potential in the whole flow domain:

$$-T_C\frac{\Delta n}{n} + \frac{T}{2}\ln\left(\frac{1+\Delta n/n}{1-\Delta n/n}\right) - \kappa_2\nabla^2\left(\Delta n\right) = constant, \quad (24)$$

$$T_C = \frac{nT}{2\Delta n_0}\ln\left(\frac{1+\Delta n_0/n}{1-\Delta n_0/n}\right), \quad (25)$$

where Δn_0 is a positive value in the component-A-rich region. Equation (24) represents the fact that under a thermodynamic equilibrium condition there is no net variation in the number of particles in each phase. Figure 2 shows examples of Δn across a flat interface calculated by using Eq.(24). As κ_2 decreases, the interface, the region where $\Delta n(x)$ changes steeply, becomes thinner and the gradient of Δn increases. Table 1 shows the value of integral in the right-hand side of Eq. (23), which are evaluated by substituting the calculated $\Delta n(x)$ into the integral. The value of σ/κ_1 decreases with increasing κ_2. This tendency can be utilized to determine the value of κ_2 to be used in a simulation. The value of κ_1 for a simulation is easily determined by substituting the value of σ and $\Delta n(x)$ into Eq.(23) and solving it for κ_1.

Table.1: Surface tension and gradient of Δn for κ_2.

κ_2	σ/κ_1	Max.$\lvert\nabla\Delta n\rvert$
0.01	0.310	0.550
0.02	0.219	0.389
0.03	0.179	0.317
0.06	0.125	0.222

To examine whether or not the above-mentioned procedure is applicable to a curved interface, the formation of a two-dimenional circular drop in stagnant liquid is simulated for several values of σ and drop diameters. Figure 3 shows the predicted pressure jump ΔP, i.e. the difference between the pressure inside the drop with radius R and the pressure outside the drop, P_0. The lines in the figure are drawn by substituting the input value of σ into the Laplace's law $\Delta P = \sigma/R$. The predicted ΔP agrees well with the Laplace's law, which verifies the validity of the proposed method of adjusting the input values of κ_1 and κ_2.

As a result of the introduction of g_a^{eq} in the convection term of Eq. (22), it becomes impossible to use the conventional translation scheme of LBM, and thereby, a finite difference-based lattice Boltzmann method (FDLBM) [14] has to be adopted as a solution scheme for Eqs. (5) and (22). The adoption of FDLBM however leads to several advantages over the conventional translation scheme such as low numerical instability for high Reynolds number problems and the applicability to arbitrary grid configuration. In this study, a third-order upwind difference scheme and the second-order Runge-Kutta's scheme are adopted for the convection term and time differencing, respectively. The kinematic viscosity ν in the 3D BF model [13] is given by

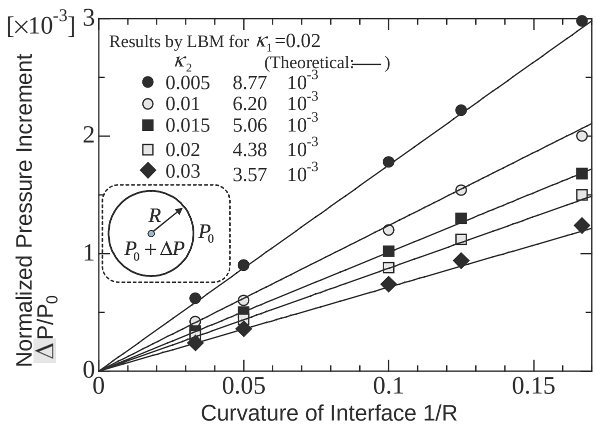

Fig.3: Pressure jump for single two-dimensional drops with various radii R.

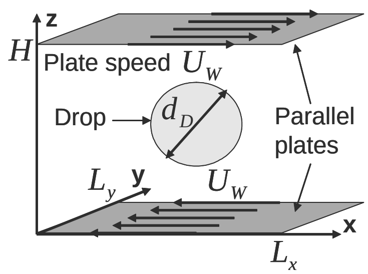

Fig.4: Intial and boundary conditions.

$$\nu = 8B_2\tau_1\, c^2. \tag{26}$$

5 NUMERICAL SIMULATION OF DROP MOTION

Numerical simulations of three-dimensional drops in a Couette flow are carried out with the proposed method. To verify the accuracy, deformation and breakup of a single drop predicted by the present method are compared with numerical predictions obtained by an advanced volume of fluid (VOF) method [10] and with an analytical solution based on a small deformation theory [11]. The initial and boundary conditions of 3D simulations are shown in Fig.4. A

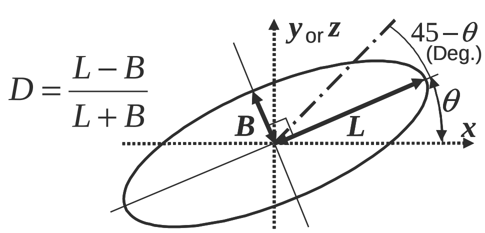

Fig.5: Measures of drop deformation and orientation.

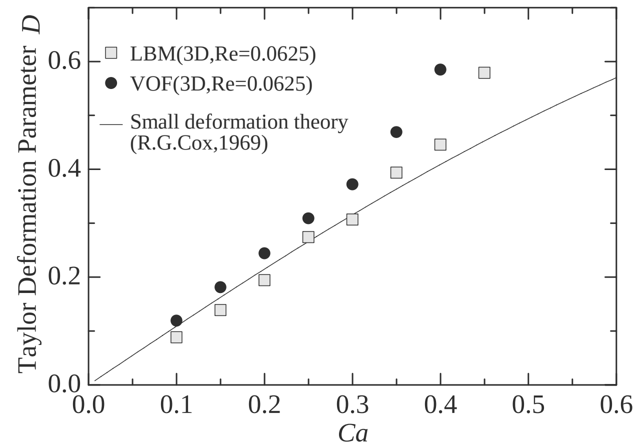

Fig.6: Taylor deformation parameter D.

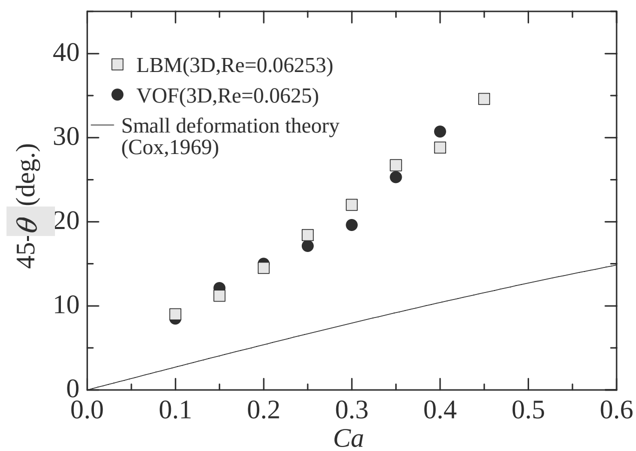

Fig.7: Drop orientation angle θ.

spherical neutrally-buoyant drop with diameter $d_D = 16$ is suspended in an immiscible liquid at the center of the computational domain. The top and bottom plates are moving at a constant speed U_W in the opposite directions. The density and viscosity of the drop are the same as those of the continuous fluid. Uniform cubic mesh, $\Delta x = \Delta y = \Delta z = 1$, is used to descretize the flow domain of plate separation H and spatial periodicities L_x and L_y. The extrapolation boundary condition proposed by Chen et al. [15] for f_a and g_a is applied to simulate the moving plates.

Simulations are carried out for several Reynolds number Re and capillary number Ca, which is the ratio of viscous force to surface tension force. These dimensionless numbers are defined by

$$Re = \frac{\dot{\gamma}}{\nu}\left(\frac{d_D}{2}\right)^2, \tag{27}$$

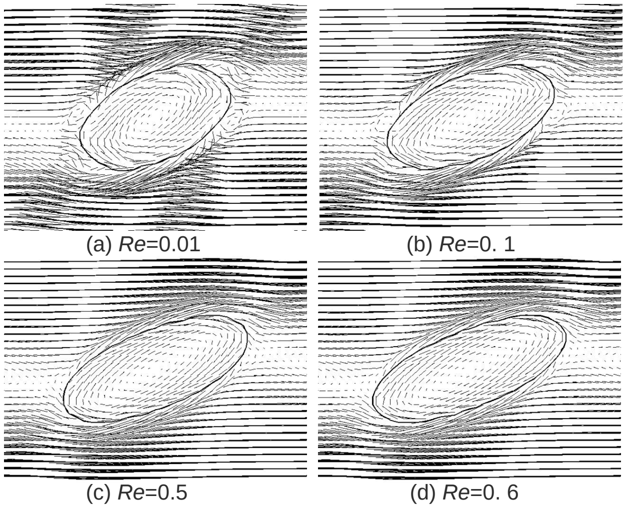

Fig.8: Predicted steady-state drop shapes and flow fields on a cross section in x-z plane across the center of drop at Ca=0.3.

$$Ca = \frac{\dot{\gamma}\,\nu\,d_D}{2\sigma}. \tag{28}$$

where $\dot{\gamma}$ is the imposed shear rate ($= 2U_W/H$).

Deformation of a drop in a time-dependent shear flow starting from a quiescent flow field is simulated under a low Reynolds number condition, $Re = 0.0625$. The dimensions are specified as $H = 128$, $L_x = 64$ and $L_y = 32$. For the quantitative comparison, two parameters are used to measure the magnitude of deformation. The one is the Taylor deformation parameter $D = (L-B)/(L+B)$, where L and B are the lengths of major and minor axes as shown in Fig.5. The other is the orientation angle θ of the major axis with respect to the axis of shear strain. The values of D and θ in a steady state, which is achieved after transient deformation, are compared with the VOF predictions and theory. Results are shown in Figs. 6 and 7. The predicted D agrees well with VOF predictions. In addition, it agrees with the small deformation theory when D is small. As for the orientation angle, good agreements are obtained between the BF model and VOF method. However the theory does not agree with both simulations.

Then breakup of a 3D drop is simulated using $d_D = 16$, $H = L_x = 64$ and $L_y = 32$. Simulations are carried out by increasing Re under a constant Ca to find a critical value of Re at which breakup takes place. Figure 8 is examples of predicted flow fields on the $x - z$ cross section at $y = 16$ for $Ca = 0.3$ and $Re = 0.01, 0.1, 0.5$ and 0.6. As Re increases, the drop deformation becomes larger, but breakup still does not occur. As shown in Fig. 9, the breakup

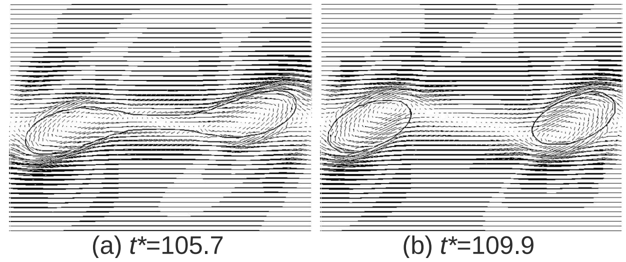

Fig.9: Snapshots of 3D drop breakup for Ca=0.3 and Re=0.75, at $t^* = t \times (2U_W/H)$.

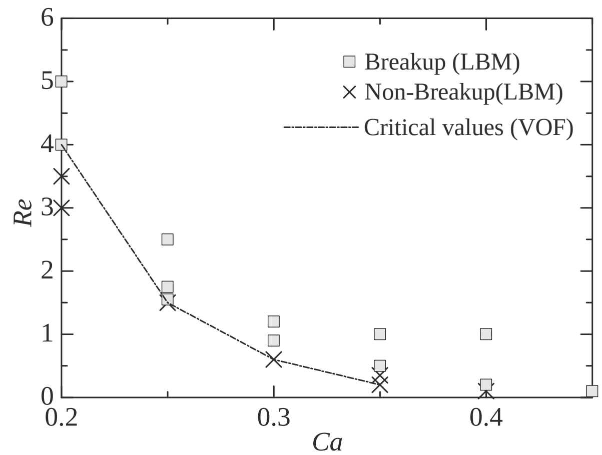

Fig.10: Diagram of drop breakup in terms of the capillary and Reynolds numbers.

takes place at $Re = 0.75$, so that the critical Re at $Ca = 0.3$ lies between 0.6 and 0.75. Figure 10 is the thus-obtained diagram of drop breakup in the (Ca, Re) plane. The critical Reynolds number predicted by VOF [10] is drawn with a solid curve. The present result again agrees well with the VOF prediction.

Then interactions of two drops in a 3D shear flow at $Ca = 0.3$ and $Re = 1.0$ are simulated using the same H, L_x, L_y and d_D as those in the breakup simulation. Note that a single drop under this combination of Re and Ca would break up. Initial conditions and snapshots of predicted flow patterns are shown in Fig. 11. In Case (a), two drops initially locate at the middle height of the domain. In this case, drops reach the steady state without breakup. This result implies that the critical Re depends on the number density of drops in a flow domain. To the contrary, when the initial heights of drops are apart from the middle elevation by d_D (Case (b)), drops deform large enough to result in breakup, which indicates that the critical Re depends not only on Ca and the number density of drops but also on the initial spatial arrangement of drops.

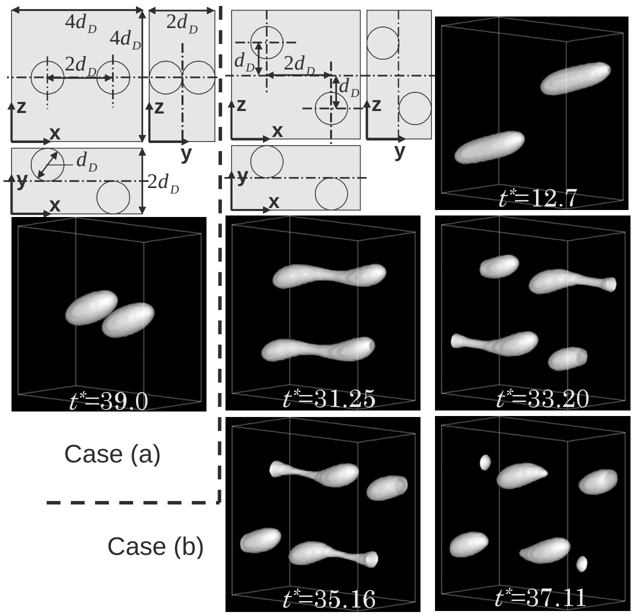

Fig.11: Initial conditions and snapshots of two-drop interaction for Ca=0.3 and Re=1.

6 CONCLUSIONS

A lattice-Boltzmann binary fluid model was improved to simulate immiscible two-phase flows with the function of easy adjustment of surface tension and interface thickness to desired values. The improvement was achieved by (a) the adoption of a particle number density function at a local equilibrium state, g^{eq} for the convection term of the lattice Boltzmann equation describing the time-evolution of number density difference between the phases and (b) the introduction of two parameters in the definition of surface free energy. The proposed method was applied to neutrally-buoyant drops in simple shear flows to examine its validity and the effects of spatial arrangement of drops on breakup process. It was confirmed that (1) deformation and breakup of single drops predicted by the proposed method agreed well with those by an advanced volume-of-fluid method and a small deformation theory, and (2) the critical Reynolds number at which drop breakup takes place depends not only on the capillary number and the number density of drops but also on the initial spatial arrangement of drops.

REFERENCES

[1] G. McNamara and G. Zanetti, Use of the Boltzmann Equation to Simulate Lattice-Gas Automata, *Phy. Rev. Lett.*, **61**, 2332 (1988).

[2] S. Chen and G. D. Doolen, Lattice Boltzmann Method for Fluid Flows, *Annu. Rev. Fluid Mech.*, **30**, 329 (1998).

[3] U. Frisch, B. Hasslacher and Y. Pomeau, Lattice-Gas Automata for the Navier-Stokes Equation, *Phys. Rev. Lett.*, **56**, 1505 (1986).

[4] M. R. Swift, W. R. Osborn and J. M. Yeomans, Lattice Boltzmann Simulation of Nonideal Fluids, *Phys. Rev. Lett.*, **75**, 830 (1995).

[5] T. Seta, K. Kono and S. Chen, Lattice Boltzmann Method for Two-Phase Flows, *Int. J. Modern Phys.*, **B 17**, 169 (2003).

[6] M. R. Swift, E. Orlandini, W. R. Osborn and J. M. Yeomans, Lattice Bolztammn Simulations of Liquid-Gas and Binary Fluid Systems, *Phys. Rev.*, **E 54**, 5041 (1996).

[7] T. Inamuro, R. Tomita and F. Ogino, Lattice Boltzmann Simulations of Drop Deformation and Breakup in Shear Flows, *Int. J. Modern Phys.*, **B 17**, 21 (2003).

[8] D. Jamet, O. Lebaique, N. Coutris and J. M. Delhaye, The Second Gradient Method for the Direct Numerical Simulation of Liquid-Vapor Flows with Phase Change, *J. Comput. Phys.*, **169**, 624 (2001).

[9] D. Jacqmin, Calculation of Two-Phase Navier-Stokes Flows Using Phase-Field Modeling, *J. Comput. Phys.*, **155**, 96 (1999).

[10] J. Li, Y. Y. Renardy and M. Renardy, Numerical Simulation of Breakup of a Viscous Drop in Simple Shear Flow through a Volume-of-Fluid Method, *Phys. Fluids*, **12**, 269 (2000).

[11] R. G. Cox, The Deformation of a Drop in a General Time-Dependent Fluid Flow, *J. Fluid Mech.*, **37**, 601 (1969).

[12] S. Chen, Z. Wang, X. Shan and G. D. Doolen, Lattice Boltzmann Computational Fluid Dynamics in Three Dimensions, *J. Stat. Phys.*, **68**, 379 (1992).

[13] N. Takada, M. Misawa, A. Tomiyama and S. Hosokawa, Simulation of Bubble Motion under Gravity by Lattice Boltzmann Method, *J. Nucl. Sci. Technol.*, **38**, 330 (2001).

[14] N. Cao, S. Chen, S. Jin and D. Martinez, Physical Symmetry and Lattice Symmetry in Lattice Boltzmann Method, *Phys. Rev. E*, **55**, 21 (1997).

[15] S. Chen and D. Martinez, On Boundary Conditions in Lattice Boltzmann Methods, *Phys. Fluids*, **8**, 2527 (1996).